T Cell-to-Stroma Enrichment (TSE) score: a gene expression metric that predicts response to immune checkpoint inhibitors in patients with urothelial cancer

Maud Rijnders[1,*], J. Alberto Nakauma-González[1,2,3,*], Debbie G.J. Robbrecht[1], Alberto Gil-Jimenez[4,5], Hayri E. Balcioglu[1], Astrid A.M. Oostvogels[1], Maureen J.B. Aarts[6], Joost L. Boormans[2], Paul Hamberg[7], Michiel S. van der Heijden[4,8], Bernadett E. Szabados[9], Geert J.L.H. van Leenders[10], Niven Mehra[11], Jens Voortman[12], Hans M. Westgeest[13], Ronald de Wit[1], Astrid A.M. van der Veldt[1,14], Reno Debets[1,*], Martijn P. Lolkema[1,*,#]

[1]Department of Medical Oncology, Erasmus MC Cancer Institute, University Medical Center Rotterdam, Rotterdam, the Netherlands
[2]Department of Urology, Erasmus MC Cancer Institute, University Medical Center Rotterdam, Rotterdam, the Netherlands
[3]Cancer Computational Biology Center, Erasmus MC Cancer Institute, University Medical Center Rotterdam, Rotterdam, the Netherlands
[4]Department of Molecular Carcinogenesis, the Netherlands Cancer Institute, Amsterdam, the Netherlands
[5]Oncode Institute, Utrecht, the Netherlands
[6]Department of Medical Oncology, GROW-School for Oncology and Reproduction, Maastricht University Medical Center, Maastricht, the Netherlands
[7]Department of Medical Oncology, Franciscus Gasthuis & Vlietland Hospital, Rotterdam/Schiedam, the Netherlands
[8]Department of Medical Oncology, the Netherlands Cancer Institute, Amsterdam, the Netherlands
[9]Barts Cancer Institute, Queen Mary University of London, London, UK
[10]Department of Pathology, Erasmus MC Cancer Institute, University Medical Center Rotterdam, Rotterdam, the Netherlands
[11]Department of Medical Oncology, Radboud University Medical Center, Nijmegen, the Netherlands
[12]Department of Medical Oncology, Amsterdam UMC, Vrije Universiteit Amsterdam, Cancer Center Amsterdam, Amsterdam, the Netherlands
[13]Department of Internal Medicine, Amphia Hospital Breda, Breda, the Netherlands
[14]Radiology & Nuclear Medicine, Erasmus MC Cancer Institute, University Medical Center Rotterdam, Rotterdam, the Netherlands

* Contributed equally
[#] Current address: Amgen Inc., Breda, the Netherlands

Corresponding author

prof. dr. Reno Debets

Dr. Molewaterplein 40, 3015 GD Rotterdam, The Netherlands

Email: j.debets@erasmusmc.nl@erasmusmc.nl

Abstract

Immune checkpoint inhibitors (ICIs) improve overall survival in patients with metastatic urothelial cancer (mUC). To identify predictive markers of response, whole-genome DNA (n=70) and RNA-sequencing (n=41) were performed using fresh metastatic biopsies prior to treatment with pembrolizumab. PD-L1 combined positivity score did not, whereas tumor mutational burden and APOBEC mutagenesis modestly predicted response. Using gene expression analysis, we defined the T cell-to-stroma enrichment (TSE) score, a signature-based metric that captures the relative abundance of T cells and stromal cells. Patients with a positive and negative TSE score show progression-free survival rates at 6 months of 67 and 0%, respectively. The TSE score was captured by immunofluorescence in tumor tissue, and validated in two independent ICI-treated cohorts of patients with mUC (IMvigor210) and muscle-invasive UC (ABACUS). In conclusion, the TSE score represents a clinically applicable marker that potentially aids in prospectively selecting patients with mUC for ICI treatment.

56 **Introduction**

57 Immune checkpoint inhibitors (ICIs) directed against programmed cell death protein
58 (PD-1) or its ligand (PD-L1) have significantly improved clinical outcomes of patients
59 with metastatic urothelial cancer (mUC). In patients with mUC with progressive disease
60 after platinum-based chemotherapy, treatment with pembrolizumab (anti-PD-1)
61 showed superior survival outcomes as compared to second-line chemotherapy in a
62 phase 3 trial[1,2]. A small subset of these patients had a durable response for >2 years[3].
63 Furthermore, first-line treatment with pembrolizumab and atezolizumab (anti-PD-L1)
64 showed efficacy in single-arm trials[4,5]. In addition, several clinical trials are currently
65 investigating the efficacy of ICIs for patients with muscle-invasive bladder cancer
66 (MIBC)[6]. Notably, the overall response rate is still limited in patients with mUC with the
67 accompanying risk of exposing non-responding patients to potential (severe) toxicities
68 and expensive therapies.

69 To date, the only biomarker available to select patients with mUC for ICIs is PD-L1
70 protein in tumor tissue. However, the predictive value of PD-L1 expression heavily
71 depends on the population of patients studied[1,4,5,7-9]. Furthermore, an important
72 limitation of PD-L1 protein is its dependence on a specific staining platform and use of
73 archival tumor tissue[10,11].

74 Another biomarker that is associated with response to ICIs is tumor mutational burden
75 (TMB)[12,13]. Recently, high TMB (≥10 mutations per mega base-pair) was approved by
76 the U.S. Food and Drug Administration as a pan-cancer measure to select patients
77 with previously treated advanced solid tumors for treatment with pembrolizumab[14,15].
78 Furthermore, immune cell infiltration[16-18], expression of immune genes such as *IFNG,*
79 *CXCL9 and CXCL10*[16,19], TGF-β signaling[20], composition of the tumor
80 microenvironment[21], alterations in DNA damage repair (DDR) genes[22], abundance of

81 circulating tumor DNA[23,24] and the diversity of the T cell receptor (TCR) repertoire[16,25,26]
82 have all been associated with response and resistance to ICIs. Other studies suggest
83 that the combination of multiple biomarkers improves response prediction for patients
84 with mUC when compared to single biomarkers[27,28]. Collectively, there is still a general
85 lack of evidence and validation of above-mentioned biomarkers in patients with mUC.

86 Along this line, we have performed whole-genome DNA-sequencing (WGS) and RNA-
87 sequencing (RNA-seq) and applied an integrative approach towards the discovery of
88 new predictors for response to ICIs in patients with mUC. We identified the T cell-to-
89 stroma enrichment (TSE) score, a transcriptomic measure comparing the expression
90 scores of signatures for T cells and stromal resident cells and their products as a robust
91 and easy to implement metric to predict response to anti-PD-1 in mUC. The predictive
92 value of this score was extended with immunofluorescence stainings, and validated in
93 two independent cohorts of patients with primary and metastatic UC treated with anti-
94 PD-L1.

Results

Patient cohort and clinical characteristics

Between March 1st 2013 and March 31st 2020, 288 patients with advanced or mUC were included according to the Center for Personalized Cancer Treatment (CPCT-02) biopsy protocol (NCT01855477; **Fig. 1**). Fresh-frozen metastatic tumor biopsies and matched normal blood samples were collected for WGS and RNA-seq as described previously[29]. Seventy patients received pembrolizumab monotherapy and were included in this analysis. Matched RNA-seq was available for 41 patients. PD-L1 combined positivity score (CPS) was assessed in biopsies of 40 patients.

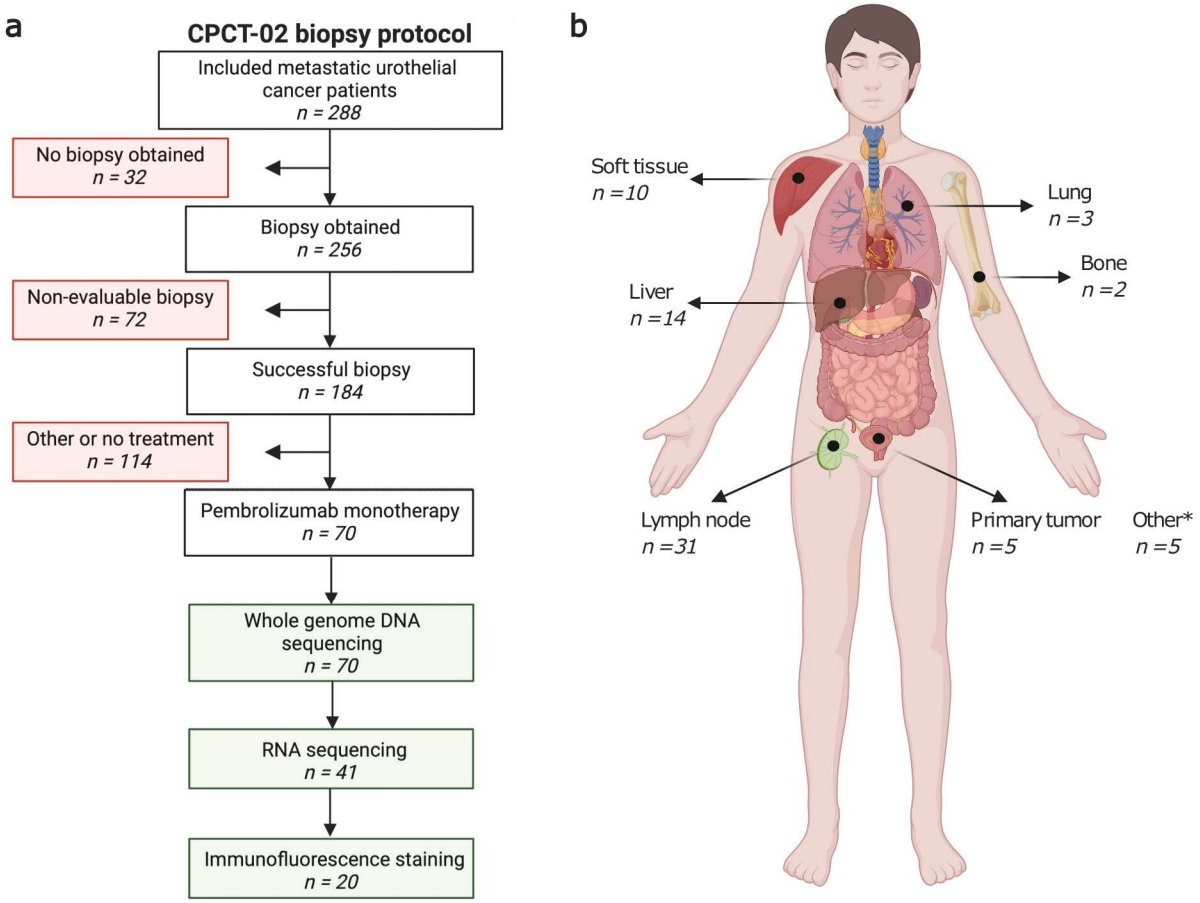

Fig. 1: Study design and biopsy sites of patients with metastatic urothelial cancer treated with pembrolizumab

(a) Flowchart of patient inclusion. Patients with advanced or metastatic urothelial cancer who were scheduled for systemic palliative treatment were selected from the prospective Center

109 for Personalized Cancer Treatment (CPCT-02) patient cohort (n=288). Patients were excluded
110 if no tumor biopsy was obtained, the biopsy was non-evaluable (tumor cell percentage <20%),
111 or in case patients were not treated with pembrolizumab monotherapy after biopsy. As a result,
112 70 patients were included for analysis. Whole-genome DNA sequencing (WGS) data were
113 available for all 70 patients. Matched RNA-sequencing data were available for 41 of these
114 patients, and tissues for immunofluorescence stainings were available for 20 of these patients.
115 (**b)** Overview of the number of biopsies per metastatic site included in this study. Primary tumor
116 samples were obtained from patients with locally advanced disease with synchronous distant
117 metastases that were not safely accessible for a biopsy. *Other biopsy sites include adrenal
118 gland (n=2), peritoneum (n=2), and local recurrence of the primary tumor (n=1). Created with
119 BioRender.com.
120

121 One-third (n=24) of patients who received pembrolizumab were responders according
122 to response evaluation criteria in solid tumors (RECIST) v1.1. The PD-L1 CPS was
123 positive (≥10) in 21% of responders and 24% of non-responders. Most patients (90%)
124 received pembrolizumab as second-line therapy, but responders more frequently
125 received pembrolizumab as first-line therapy compared to non-responders (25% *vs*
126 2%; Fisher's exact test p=0.005; chemotherapy-naïve patients were selected for a
127 positive PD-L1 CPS). At data cut-off, 27% of patients were alive. The median overall
128 survival (OS) was 8.9 months, and the median progression-free survival (PFS) was 2.9
129 months. Patient characteristics are summarized in **Supplementary Table 1**.
130

131 **TMB and APOBEC mutagenesis only modestly predict response to**
132 **pembrolizumab**

133 The majority of patients (54%) in our cohort had a high TMB (**Fig. 2)**. Of patients with
134 high TMB, 47% were responders, whereas only 19% of patients with low TMB were

135 responders (Fisher's exact test p=0.022; **Supplementary Fig. 1**). Previously, five
136 genomic subtypes (GenS) of mUC have been identified according to COSMIC v3.1
137 mutational signatures[30]. GenS1, which is related to APOBEC mutagenesis, was
138 identified in 61% of samples. Overall, genomic subtypes were not associated with
139 treatment response. Of patients with high APOBEC mutagenesis (n=29), 48%
140 responded to pembrolizumab, whereas 24% of patients with non-high APOBEC
141 mutagenesis (n=41) responded to pembrolizumab (Fisher's exact test p=0.045;
142 **Supplementary Fig. 1**). One responder had no evidence of APOBEC mutagenesis
143 but had a high TMB as a result of defective DNA mismatch repair. We did not observe
144 differences between responders and non-responders with respect to HR deficiency nor
145 presence of chromothripsis.

146 Furthermore, when evaluating the presence of driver gene alterations, we did not
147 observe statistically significant differences between responders and non-responders
148 (**Supplementary Fig. 2**). Alterations in canonical signaling pathways were most
149 frequently observed in the p53, cell cycle, and RTK-RAS pathways (**Supplementary**
150 **Fig. 3a; Supplementary Data 1**), yet not significantly different between the two patient
151 groups. Also, the frequency of alterations in DDR genes and signaling pathways was
152 not statistically different between responders and non-responders (**Supplementary**
153 **Fig. 3b**). Activity of the p53 pathway was reduced in those patients (responders and
154 non-responders alike) with genomic alterations in this pathway (**Supplementary Fig.**
155 **3c**). Collectively, the genomic analyses revealed only modest predictive value of TMB
156 and APOBEC mutagenesis for response to anti-PD-1.

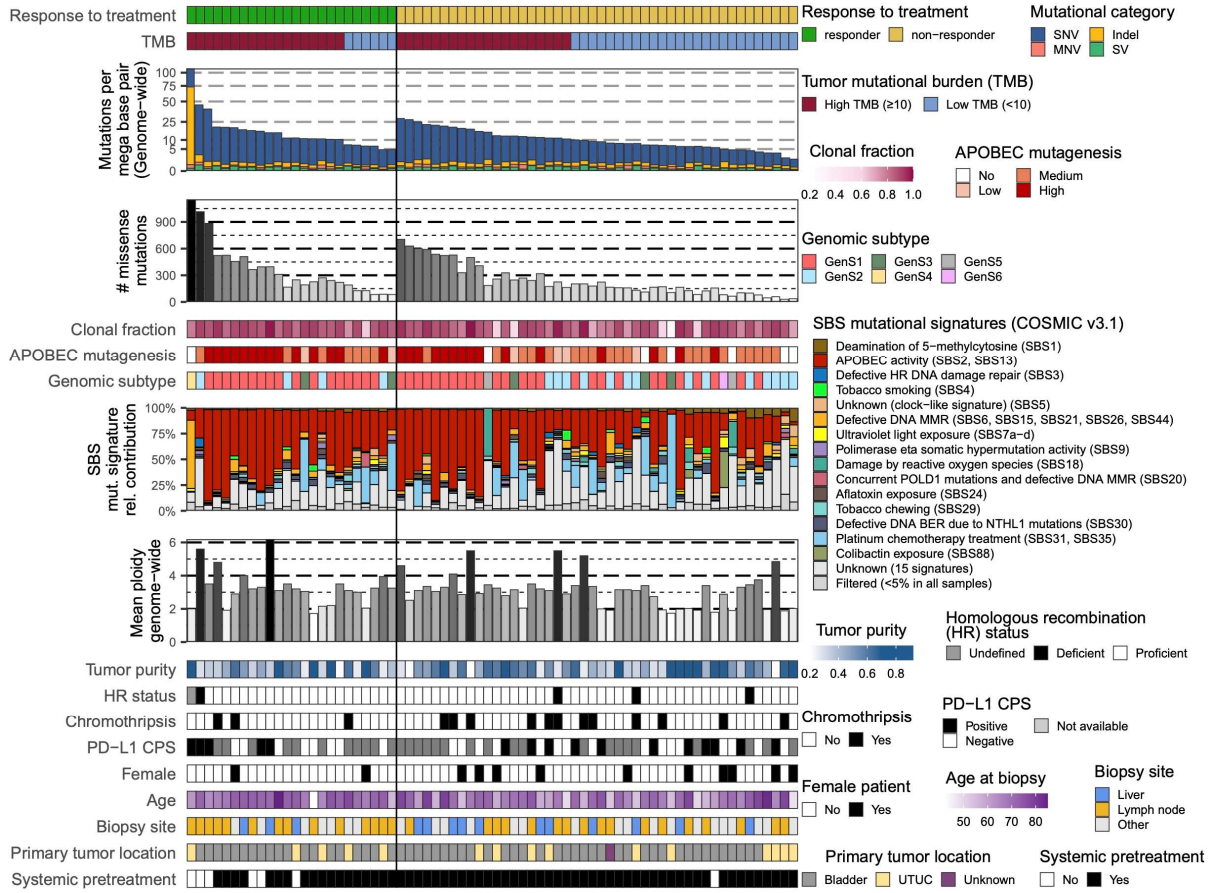

Fig. 2: The genomic landscape of patients with metastatic urothelial carcinoma treated with pembrolizumab

Whole-genome sequencing data from biopsy samples of patients with metastatic urothelial carcinoma (n=70) are displayed according to treatment response at 6 months of therapy (responder: ongoing complete or partial response, or stable disease, n=24; non-responder: progressive disease, n=46). Genomic and clinical features are listed from top to bottom as follows: genome-wide tumor mutational burden (TMB), and classification into high and low; total number of missense mutations; clonal fraction of mutations; APOBEC enrichment analysis showing tumors with no-, low-, medium- and high-APOBEC mutagenesis; genomic subtypes according to mutational signatures[30]; single base substitution (SBS); mutational signatures according to COSMIC v3.1; genome-wide mean ploidy; tumor purity; homologous recombination (HR) status; tumors with at least one chromothripsis event; PD-L1 combined positivity score (CPS) according to the companion diagnostic assay of pembrolizumab

171 (positive: CPS≥10, negative: CPS<10, or not available (NA)); female patients; age at time of
172 biopsy; metastatic site from which a biopsy was obtained; primary tumor location (bladder or
173 upper tract urothelial carcinoma, UTUC); and patients who received systemic treatment prior
174 to start of anti-PD-1 therapy.

175

176 **Expression of genes representing immune cells and stromal cells distinguishes**
177 **responders from non-responders to pembrolizumab**

178 Differential gene expression analysis of RNA-seq data (n=41) revealed that up-
179 regulated genes in responders *vs* non-responders were part of a chemokine pathway,
180 and a pathway related to interactions between lymphoid and non-lymphoid cells (**Fig.**
181 **3**). Down-regulated pathways in responders (up-regulated in non-responders) were
182 related to extracellular matrix organization and collagen formation, generally linked to
183 the activity of stromal cells. An example of an up-regulated pathway in responders
184 involved interleukin-10 (IL-10), a recognized immunosuppressor, which in recent
185 studies has also been associated with T cell activation in solid tumors[31]. Since IL-10
186 can be expressed by several cell types, including cancer cells, the origin as well as the
187 exact functioning of IL-10 in the context of ICI treatment requires further investigation.

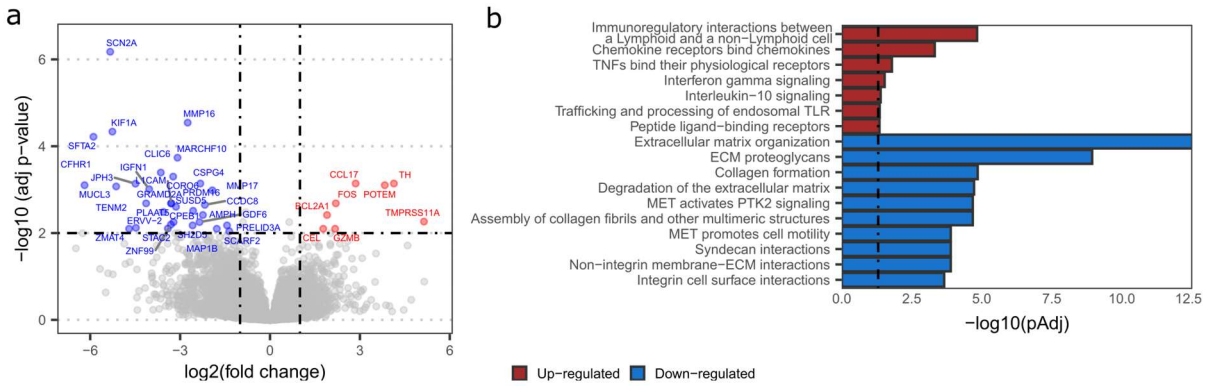

Fig. 3: Differential expression of genes and pathways related to immune cell and stromal cell activity for responders and non-responders to pembrolizumab

(a) Volcano plot showing genes with up-regulated or down-regulated expression in responders (n=13) *vs* non-responders (n=28). Genes of which differential expression analysis showed adjusted p<0.01 and absolute log2 fold change >1 are labelled in red (up-regulated) and blue (down-regulated). (**b)** Bar diagrams specify the pathways of differentially expressed genes according to ReactomePA v1.34.0[41]. Enriched pathways with adjusted p<0.05, indicated by the vertical dashed line, were considered significant. All significantly up-regulated pathways, and the top ten down-regulated pathways are displayed.

Patient stratification according to T cell-to-stroma enrichment score coincides with response to pembrolizumab

Following up on the pathway analysis displayed in **Fig. 3**, we have interrogated the transcriptomic landscape of our cohort for a broad list of gene signatures related to T cells, other (non-T cell) immune cells, and stromal cells and their products (see **Supplementary Table 2** for a detailed overview of gene signatures). Some of these signatures have been reported as predictors of response and resistance to ICIs[18,20]. Hierarchical clustering according to the complete set of signatures revealed three distinct patient clusters (**Fig. 4**). In cluster one (n=18), 61% of patients showed a response to pembrolizumab. These patients predominantly had high signature scores

209 for T cells and other immune cells. In cluster two (n=10), 20% of patients showed a
210 response to pembrolizumab. These patients generally had a similar score for all
211 signatures, independent of the cell type(s) and products they represented. In cluster
212 three (n=13), none of the patients showed a response to pembrolizumab. These
213 patients predominantly had high signature scores for stromal cells and their products.
214 The above clustering suggested that signature scores for immune cells and stromal
215 cells and their products were related to response to pembrolizumab. To select those
216 signatures with the most predictive value, ROC curves were constructed per signature,
217 which demonstrated areas under the curve (AUC) that ranged from 0.54 to 0.77
218 (median = 0.68; **Supplementary Table 3**). The highest AUCs (>0.7) were observed
219 for T cells and stromal cells and their products, and (non-T cell) immune cells showed
220 AUCs below the median. Signatures that showed the highest discriminatory power
221 were selected and combined into either a global T cell or a global stromal signature
222 (**Supplementary Fig. 4**). Notably, logistic regression analyses showed that the global
223 T cell signature was an independent predictor of response (Coefficient=3.03, p=0.005),
224 while the global stromal signature was an independent predictor of non-response
225 (Coefficient=-2.40, p=0.010) to pembrolizumab. Next, we combined these two global
226 signatures into a single metric that we termed the T cell-to-stroma enrichment (TSE)
227 score and that reflects the abundance of T cells relative to that of stromal cells and
228 their products. This TSE score revealed a significantly higher predictive value
229 (AUC=0.88) for treatment response than either global or individual signatures alone
230 (**Supplementary Table 3**). Stratifying patients by their TSE score resembled the
231 patient groups obtained by hierarchical clustering and revealed almost identical
232 response rates (67%, 21% and 0% for patients with a positive, neutral or negative TSE
233 score).

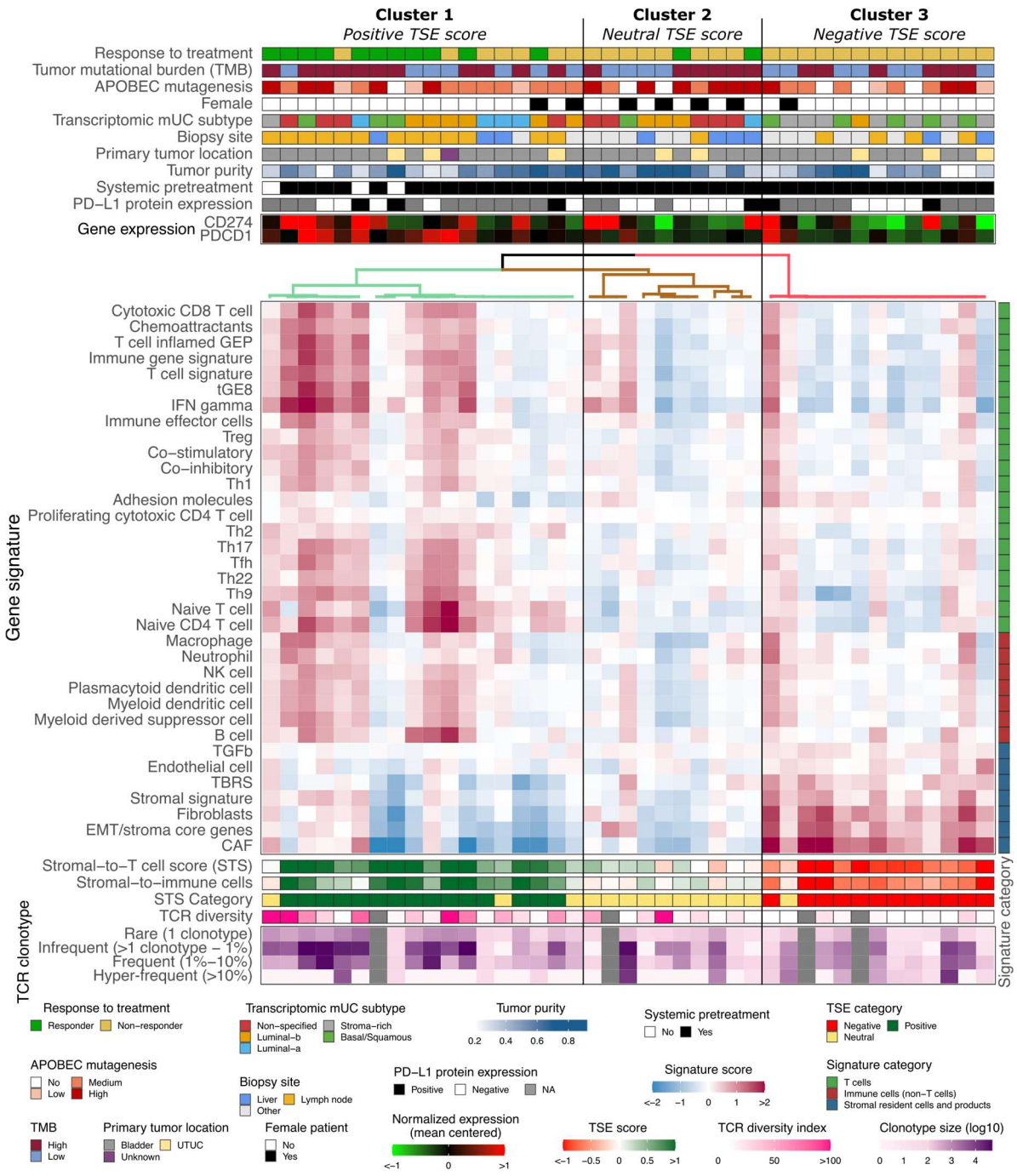

Fig. 4: Hierarchical clustering of gene signatures representing T cells, immune cells and stromal cells and their products distinguishes responders from non-responders to pembrolizumab

Transcriptomic profile of 41 patients with metastatic urothelial carcinoma (mUC), clustered using ConsensusClusterPlus v1.54.0[42] according to gene signature scores. Transcriptomic and clinical features are listed from top to bottom as follows: response to treatment at 6 months

241 of therapy (responder: ongoing complete or partial response, or stable disease, n=13; non-
242 responder: progressive disease, n=28); tumor mutational burden (TMB) classified into high
243 and low; APOBEC enrichment analysis showing tumors with no-, low-, medium- and high-
244 APOBEC mutagenesis; transcriptomic subtypes of mUC[30]; biopsy site; primary tumor location
245 (bladder or upper tract urothelial carcinoma, UTUC); tumor purity; patients who received
246 systemic treatment prior to start of anti-PD-1 therapy; PD-L1 combined positivity score (CPS;
247 positive: CPS≥10, negative: CPS<10, or not available (NA)); *CD274* (PD-L1) and *PDCD1* (PD-
248 1) gene expression; expression score for reported gene signatures related to T cells, immune
249 cells (non-T cells), and stromal cells and their products; T cell-to-stroma enrichment (TSE)
250 score; categories of the TSE score (positive, neutral or negative); T cell receptor (TCR)
251 diversity index and clonotype sizes.
252
253 It is noteworthy that patients with a positive TSE score were enriched for biopsies from
254 lymph nodes (Fisher's exact test p<0.001). When the analysis was restricted to only
255 samples from lymph nodes (n=18), the predictive value of the TSE score reached
256 similar statistics as for the whole cohort (Fisher's exact test p=0.02; **Supplementary**
257 **Fig. 5**), demonstrating the robustness of the TSE score. Patients with a neutral TSE
258 score were enriched for females (Fisher's exact test p=0.004), whereas other
259 characteristics such as age (Kruskal-Wallis test by ranks, p=0.64) and pre-treatment
260 status (Fisher's exact test p=0.54) did not correlate with the TSE score categories. The
261 vast majority of tumors with a negative TSE score (92%) were classified as stroma-
262 rich or basal/squamous according to the transcriptomic subtypes of mUC[30]. TMB and
263 APOBEC mutagenesis were not different between the three TSE score groups (**Fig.**
264 **4**). Likewise, the distribution of driver gene alterations, hotspot mutations and gene
265 fusions were similar across TSE score groups (**Supplementary Fig. 6**). Also, PD-L1
266 CPS was similar across the TSE score groups (**Fig. 4**), whereas *CD274* (PD-L1) and

267 *PDCD1* (PD-1) gene expressions were higher for patients with a positive *vs* negative
268 TSE score (**Supplementary Fig. 7**). When assessing the relative abundance of
269 immune cell populations, we observed that the fraction of myeloid dendritic cells was
270 higher in patients with a positive *vs* negative TSE score (**Supplementary Fig. 8-9**).
271 Furthermore, the TCR diversity and the relative abundance of less frequent TCR
272 clonotypes was higher in patients with a positive *vs* negative TSE score (**Fig. 4,**
273 **Supplementary Fig. 8, Supplementary Fig. 10**).
274

275 **The TSE score is a superior predictor for response and survival compared to**
276 **genomic metrics**

277 To evaluate the predictive values of the TSE score, TMB, APOBEC mutagenesis and
278 their combinations for response to pembrolizumab, ROC curves were analyzed (**Fig.**
279 **5a**). The TSE score was superior to TMB or APOBEC mutagenesis to identify
280 responders from non-responders (**Fig. 5a**; DeLong's test p=0.006 and p=0.003 for
281 AUC of TSE score *vs* TMB and APOBEC mutagenesis, respectively). The AUC of the
282 TSE score did not improve when combined with TMB and/or APOBEC mutagenesis.
283 Furthermore, patients with a positive TSE score had a longer overall survival (OS) and
284 progression-free survival (PFS) when compared to other patients (**Fig. 5b)**.
285 Multivariate cox regression analysis, using continuous values, showed that the TSE
286 score had a superior predictive value for OS (TSE score p<0.001; TMB p=0.21;
287 APOBEC p=0.25) and PFS (TSE score p=0.002; TMB p=0.32; APOBEC p=0.27) than
288 TMB and APOBEC mutagenesis (**Fig. 5b-d)**.

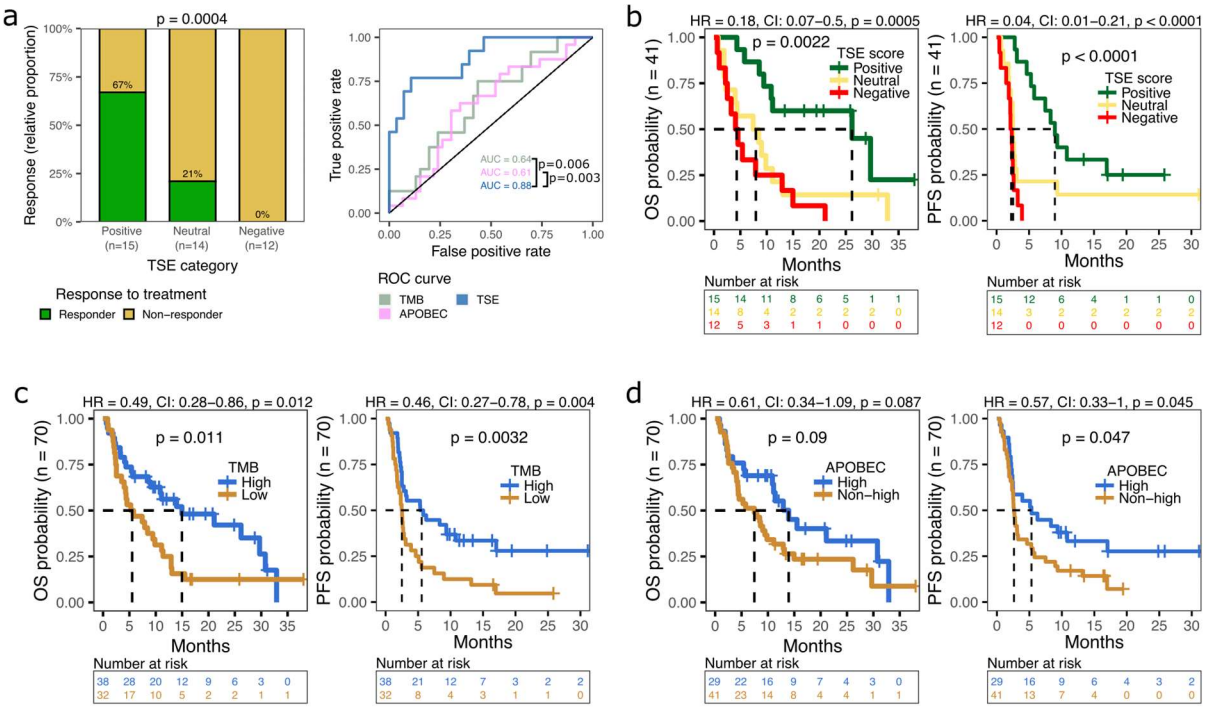

Fig. 5: Association of the TSE score, TMB and APOBEC mutagenesis with response to pembrolizumab and overall and progression-free survival

(a) Bar graphs display the relative proportion of responders and non-responders in patients with a positive, neutral, or negative TSE score (TSE positive, n=15; TSE neutral, n=14; TSE negative, n=12). P-value of TSE positive *vs* negative was determined using the Fisher's exact test. Receiver operating characteristic (ROC) curves of TSE score, TMB, APOBEC mutagenesis (enrichment for APOBEC-associated mutations), and their combinations were constructed using continuous variables. The area under the curve (AUC) is displayed per condition, and p-values reflect DeLong's test of AUC's. (**b)** Overall survival (OS) and progression-free survival (PFS) probability in patients with a positive, neutral or negative TSE score; **(c)** high (n=38) or low (n=32) TMB; or (**d)** high (n=29) or non-high (n=41) APOBEC mutagenesis. Log-rank test was applied to survival curves. For TSE score, hazard ratio (HR) was calculated for positive *vs* negative. CI = confidence interval.

In extension to the transcriptomic analysis, we evaluated the TSE score at protein level. To this end, we performed immunofluorescence stainings to visualize and quantify

306 CD4 and CD8 T cells as well as fibroblast activating protein (FAP) and podoplanin
307 (PDPN) as stromal products (see Materials and Methods for details) using 20 samples
308 with matched RNA-seq data (**Fig. 6, Supplementary Fig. 11**). In tumor tissues, CD4
309 and CD8 T cell markers (present in TSE-positive; nearly absent in TSE-negative
310 samples) showed an inverse relationship with PDPN expression (nearly absent in TSE-
311 positive; present in TSE-negative samples) (**Fig. 6a**, **Supplementary Fig. 11a-b**).
312 When calculating a protein-based metric according to the TSE-RNA score, we
313 observed that the TSE-protein score correlates well with its RNA-based counterpart
314 (**Fig. 6b**). Finally, we confirmed that combining the protein markers for T cells and
315 stromal products into a single metric improves prediction for response to
316 pembrolizumab **(Fig. 6b, Supplementary Fig. 11c-e**).

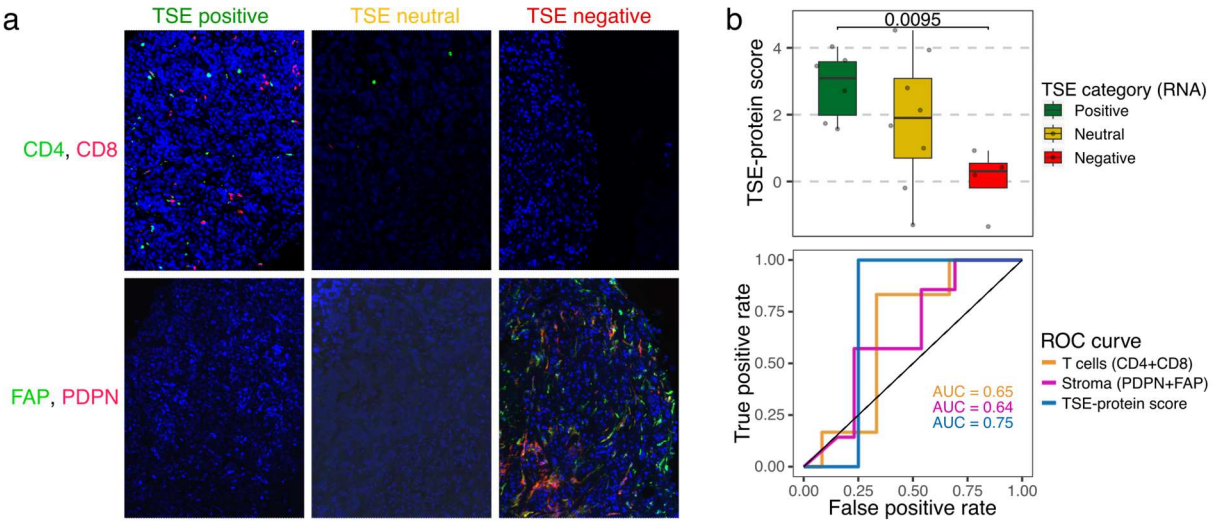

317

318 **Fig. 6: Immunofluorescence staining of T cell and stromal markers capture the TSE**
319 **score**

320 **(a)** Representative images of immunofluorescence staining for two T cell markers (CD4 and
321 CD8 T cells) and two markers of stromal resident cells and their products (FAP and PDPN)
322 according to the T cell-to-stroma enrichment (TSE) score (TSE positive, n=7; TSE neutral, n=8;
323 TSE negative, n=5). **(b)** The TSE-protein score was calculated from the densities of the four
324 markers from (a) in analogy to the TSE-RNA score; see Materials and Methods for details.

325 *Upper plot*: box plot displaying the TSE-protein score in patients with a positive, neutral, or
326 negative TSE-RNA score. *Lower plot*: receiver operating characteristic (ROC) curves of T cell
327 markers, stromal markers and the TSE-protein score. The area under the curve (AUC) is
328 displayed per condition.
329

330 **The TSE score as a predictor for response to pembrolizumab was validated in**
331 **independent cohorts of patients with urothelial cancer**

332 To substantiate the predictive value of the TSE-RNA score for response to ICIs, and
333 its potential clinical applicability, we set out to validate this score in two independent
334 cohorts of UC patients from the IMvigor210[20] (n=348) and ABACUS[18] (n=84) trials. The
335 IMvigor210 trial evaluated the efficacy of atezolizumab (anti-PD-L1) in patients with
336 platinum-refractory locally advanced or mUC. The TSE score was predictive for
337 response (based on best overall response according to RECIST v1.1) to anti-PD-L1 in
338 this cohort. It is noteworthy that for this trial the AUC of the TSE score (AUC=0.65) was
339 similar to the AUC of TMB (AUC=0.71). Patients with a positive TSE score had a higher
340 response rate (36%) than patients with a neutral (18%) or negative (13%) TSE score.
341 A longer OS was observed in patients with a positive TSE score when compared to
342 other patients (Fisher's exact test p<0.001) (**Fig. 7a**). Interestingly, among non-
343 responders in this trial, there was an enrichment for a negative TSE score in pre-
344 treated (30/59) *vs* treatment-naïve (9/37) patients (Fisher's exact test p=0.01;
345 **Supplementary Fig. 12**), which implies that the micro-milieu of tumors has evolved
346 towards relative T cell deficiency as a consequence of pre-treatment. The ABACUS
347 trial evaluated the efficacy of neoadjuvant treatment with atezolizumab in patients with
348 MIBC. Again, the TSE score was predictive for response (based on a pathological
349 complete response (pCR) at cystectomy) in the second validation cohort. In the
350 ABACUS cohort, TMB failed to predict response to neoadjuvant treatment[18], and the

AUC for the TSE score (AUC=0.74) was higher than the AUC of TMB (AUC=0.51). The pCR rate was 44% for patients with a positive TSE score and was higher when compared to patients with a negative TSE score (9%, Fisher's exact test p=0.009). In addition, patients with a positive TSE score experienced a longer recurrence-free survival (**Fig. 7b**). Together, these results suggest that contrary to TMB or ABOPEC mutagenesis, the TSE score is a robust marker that predicts response to anti-PD-1 as well as anti-PD-L1 in both metastatic and primary UC.

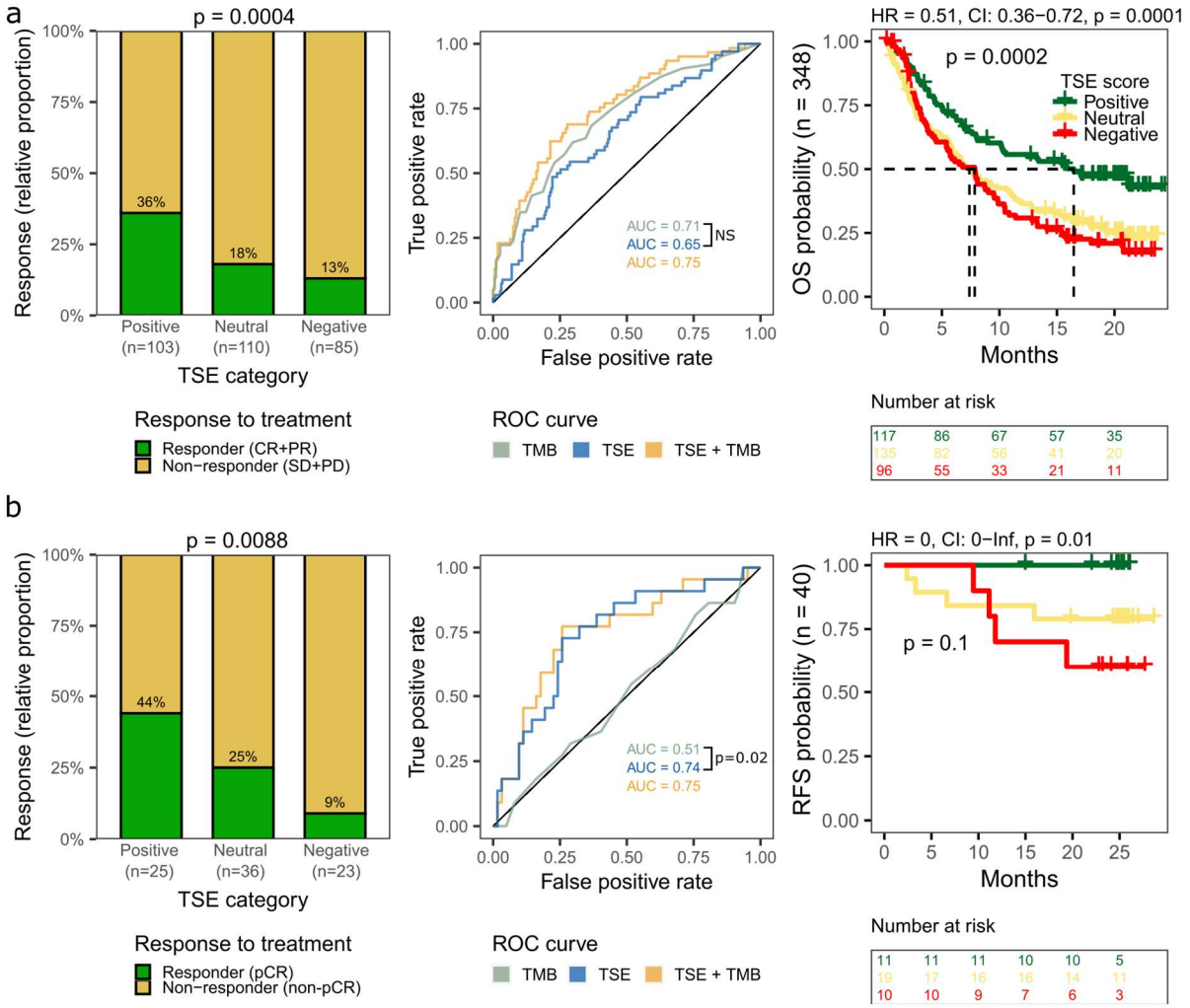

Fig. 7: Predictive value of the TSE score for response to ICIs in two independent cohorts of patients with urothelial carcinoma

Validation of the T cell-to-stroma enrichment (TSE) score in the **(a)** IMvigor210 cohort (n=348) and the **(b)** ABACUS trial (n=84). *Left graphs:* The bar graphs display the relative proportion

363 of responders and non-responders in patients with a positive, neutral, or negative TSE score.
364 In the IMvigor210 cohort (n=298 response to treatment available), responders were defined as
365 those patients with a complete response (CR) or partial response (PR), and non-responders
366 as those with stable disease (SD) or progressive disease (PD) as best overall response
367 according to RECIST v1.1. In the ABACUS trial, responders were patients with a pathological
368 complete response (pCR) at cystectomy. Fisher's exact test was applied on the proportion of
369 responders in patients with a positive *vs* negative TSE score. *Middle graphs:* Receiver
370 operating characteristic (ROC) curves of the TSE score, tumor mutational burden (TMB) and
371 their combination. P-values reflect DeLong's test of area under the curve (AUC) generated for
372 the TSE score *vs* TMB (NS=not significant). *Right graphs:* Overall survival (OS) probability was
373 available for all patients in the IMvigor210 cohort and recurrence-free survival (RFS) was
374 available for 40 patients in the ABACUS cohort. Log-rank test was applied to survival curves.
375 Hazard ratios (HR) were calculated for patients with a positive *vs* negative TSE score. CI =
376 confidence interval.
377

378 **Discussion**

379 In this study, we aimed to identify a marker or metric that predicts response to
380 pembrolizumab by analyzing the genomic and transcriptomic profiles of metastatic
381 lesions from patients with mUC prior to treatment. We observed that gene expression
382 signatures of T cells or stromal cells and their products associated with either response
383 or resistance to pembrolizumab. We translated these findings into the TSE score, a
384 single and novel transcriptomic metric that captures individual and already recognized
385 gene signatures related to abundance of T cells and stromal cells and their products.
386 This TSE score acted as a superior predictor for response and survival when compared
387 to alternative markers, and this score was not confounded by metastatic site.
388 Furthermore, the predictive value of the TSE score was supported by
389 immunofluorescence stainings in tumor tissue, and was validated in two independent
390 cohorts of patients with primary and metastatic urothelial cancer treated with anti-PD-
391 L1.

392 In line with previous studies in patients with mUC[13,16,25,26], high TMB and high APOBEC
393 mutagenesis were associated with response to pembrolizumab in our cohort. However,
394 the predictive value of both genomic scores was limited since approximately 20% of
395 patients with low TMB or non-high APOBEC mutagenesis still had benefit from
396 treatment. PD-L1 CPS failed to predict outcome in our cohort, although we cannot
397 exclude that the analysis may have been underpowered, as other studies have shown
398 a link between PD-L1 CPS and response to immunotherapy[11]. Analysis of
399 transcriptomics revealed that expression of genes representing immune cells and
400 stromal cells distinguishes responders from non-responders to pembrolizumab,
401 particularly those that were part of chemotaxis, interactions between lymphoid and
402 non-lymphoid cells, and extracellular matrix organization. The TSE score, taken into

403 account signatures that capture T cells and stromal cells and their products, resulted
404 in a better predictive value when compared to TMB, APOBEC or single gene
405 signatures. In fact, the majority of patients with a positive TSE score responded to
406 pembrolizumab and patients had superior OS and PFS when compared to other
407 patients. In contrast, none of the patients with a negative TSE score had a response
408 to treatment. At the transcriptomic level, tumors with a negative TSE score were
409 characterized by signatures related to TGF-β signaling and epithelial-to-mesenchymal
410 transition (EMT), and most of these tumors were of the stroma-rich or basal-squamous
411 mUC subtype. A negative TSE score may reflect an immune-evasive state limiting T
412 cell influx and migration caused by an overly active stromal compartment. Indeed,
413 TGF-β signaling has previously been associated with an immune excluded phenotype,
414 and a fibroblast and collagen-rich tumor stroma in anti-PD-L1 resistant mUC[20]. In
415 addition, in patients with mUC treated with anti-PD-1, EMT-like gene expression by
416 stromal cells was shown to be related to treatment resistance, even in the presence of
417 T cell infiltration[32]. Moreover, the association between non-response as well as poor
418 survival and a fibrotic subtype of the tumor micro-environment has been observed in
419 patients with mUC and other cancers[21].

420 Early studies have shown an association between TCR repertoire and response to
421 ICI[33,34]. In the current study, we found that patients with a positive TSE score showed
422 higher TCR diversity and higher abundance of infrequent TCR clonotypes, whereas
423 patients with a negative TSE score showed higher abundance of hyper-frequent TCR
424 clonotypes. These data support the notion that in tumor tissues with higher abundance
425 of T cells over stromal resident cells, and consequently more contact areas between T
426 cells and tumor cells, T cell expansion would easily occur and result in a relative
427 dominance of infrequent TCR clones (as dictated by antigens expressed by the

428 tumors). In contrast, in tumor tissues with higher abundance of stromal resident cells
429 over T cells, T cell expansion would be restricted, which, given the low total size of
430 TCR clones, would yield a relative dominance of hyper-frequent TCR clones. In
431 addition, samples with a positive TSE score contained a higher fraction of dendritic
432 cells when compared to samples with a negative TSE score. This finding extends our
433 previous study where we reported the clustering of myeloid cells and T cells in
434 metastatic lesions of patients who responded but not patients who did not respond to
435 anti-PD1[35].

436 The TSE score was visualized and tested at the protein level by staining for T cell
437 markers and stromal products. When calculating a protein-based TSE metric, we again
438 observed clear predictions for response to pembrolizumab. These findings support the
439 TSE score as a transcriptomic metric, not excluding the potential clinical application of
440 the TSE-protein score, which would require additional studies into the most optimal
441 combination of protein markers and their cut-offs to stratify patients according to TSE-
442 protein categories. Furthermore, the TSE score was validated in two independent
443 patient cohorts, namely patients with mUC treated with atezolizumab (IMvigor210 trial)
444 and patients with MIBC treated with neo-adjuvant atezolizumab (ABACUS trial). The
445 TSE score was able to predict response to atezolizumab in both cohorts, and was
446 associated with improved survival. We also utilized the IMvigor210 cohort to assess
447 whether response prediction according to the TSE score is related to pre-treatment.
448 We observed that non-responders who had received platinum-based chemotherapy
449 were enriched for a negative TSE score when compared to those patients who had not
450 received pre-treatment. This suggests that platinum-based chemotherapy induced a
451 micro-environmental shift towards less T cells and/or more stromal resident cells, and
452 adversely impacts response to ICI as a second-line therapy, and warrants confirmative

453 analyses using paired samples before and after chemotherapy. The predictive value
454 of the TSE score for OS in the IMvigor210 cohort appeared less strong compared to
455 our cohort. Possibly this can be explained by differences between the two cohorts with
456 respect to sample collection, definition of response to treatment, and/or timing of tumor
457 tissue collection relative to treatment initiation. In the ABACUS cohort, and in line with
458 the current cohort, tissue samples were obtained directly prior to therapy initiation and
459 may therefore better reflect the transcriptomic state of the tumor, suggesting that fresh
460 biopsies may improve the predictive power of the TSE score. Importantly, based on
461 the findings from the ABACUS cohort, the TSE score seems to be applicable beyond
462 the metastatic setting, confirming the robustness of the TSE score as a predictor for
463 response to ICIs in patients with urothelial cancer. A limitation of the current study is
464 the relatively small cohort size, which reduced our statistical power to further improve
465 the stratification of patients within the TSE score groups. More specifically, the group
466 of patients with a neutral TSE score showed a response rate of approximately 20% in
467 all three independent cohorts. Identifying responders within this group using genomics,
468 transcriptomics and other molecular markers, would be necessary to improve the
469 selection of these patients for ICIs.

470 In conclusion, analysis of the transcriptome and supported by immune stainings
471 identified the TSE score as a clinically relevant marker to select patients with UC for
472 PD-(L)1-targeting ICIs, both in the primary and metastatic setting. Since a negative
473 TSE score identifies patients who will not derive benefit from treatment with PD-(L)1-
474 targeting ICIs, future studies are warranted to adapt treatment for these patients in
475 order to improve outcomes.

476 **Methods**

477 **Patient cohort and study design**

478 Between March 1st 2013 and March 31st 2020, patients with advanced or mUC from
479 31 Dutch hospitals were included in the nationwide Center for Personalized Cancer
480 Treatment (CPCT-02) biopsy protocol (NCT01855477). The study protocol was
481 approved by the medical ethics review board of the University Medical Center Utrecht,
482 the Netherlands. Written informed consent was obtained from all participants prior to
483 inclusion in the trial. The study population consisted of 288 patients who were
484 scheduled for 1st or 2nd line palliative systemic treatment. Fresh-frozen metastatic
485 tumor biopsies and matched normal blood samples were collected from 256 patients
486 as described previously[29]. WGS was successfully performed for 184 patients. Seventy
487 patients started a new line of pembrolizumab monotherapy and were included in the
488 current analysis. Matched RNA-seq was available for 41 patients, and
489 immunofluorescence stainings were performed for 20 of these patients. WGS, RNA-
490 seq and clinical data are available through the Hartwig Medical Foundation at
491 https://www.hartwigmedicalfoundation.nl, under request number DR-176. A summary
492 of all genomic, transcriptomic and immunofluorescence staining results as well as
493 clinical data and response to treatment are available in **Supplementary Data 2**.

494

495 **Treatment and assessment of response**

496 Patients were treated with pembrolizumab, 200 mg intravenously every 3 weeks, or
497 400 mg every 6 weeks. Tumor response evaluation was performed using computed
498 tomography every 12 weeks. Treatment response was measured according to
499 response evaluation criteria in solid tumors (RECIST) v1.1. Data cut-off was set at July
500 1st, 2020, resulting in a minimal follow-up of 6 months for all patients with a response

501 to treatment. Response was assessed at 6 months of therapy and patients were
502 classified as responder when they showed ongoing complete or partial response, or
503 stable disease. Patients were classified as non-responder when they had progressive
504 disease within six months after treatment initiation. Patients treated beyond initial
505 radiological disease progression were classified according to the date of their first
506 radiological progression event.
507

508 **PD-L1 immunohistochemistry and scoring**

509 PD-L1 expression was assessed on metastatic tumor biopsies (paraffin embedded)
510 that were freshly obtained prior to start of pembrolizumab (n=32) using the companion
511 diagnostic assay of pembrolizumab (PD-L1 IHC 22C3 pharmDx, Agilent Technologies,
512 Carpinteria, CA, USA). When no fresh tumor biopsy was available, archival tumor
513 tissue (primary tumor or metastasis) was used (n=8). All tissues were assessed for the
514 PD-L1 combined positivity score (CPS) by an expert genitourinary pathologist
515 (GJLHvL).
516

517 **Whole-genome sequencing and analysis**

518 Alignment and pre-processing of WGS data, including the estimation of tumor purity
519 (PURPLE v2.49), were performed using tools developed by the Hartwig Medical
520 Foundation (https://github.com/hartwigmedical/hmftools)[29]. Subsequent detection of
521 driver genes, mutational signatures, genomic subtypes, homologous recombination
522 (HR) deficiency, structural variants, chromothripsis events and apolipoprotein B
523 mRNA-editing enzyme, catalytic polypeptide-like (APOBEC) mutagenesis have been
524 previously described[30,36]. APOBEC-enriched tumors were classified as high when
525 enrichment (E) for APOBEC-related mutations was $E \geq 3$, medium when $2 \leq E < 3$ and low

526 when $E<2$. The transcriptomic subtype of each sample was identified as a result of the
527 highest ranked association between the mean (normalized) expression of all genes
528 and a particular subtype across all subtypes[30]. The clonal fraction of mutations was
529 estimated as previously described[37]. In this study, mutations were considered clonal
530 when the variant copy number was >0.75.

531

532 **RNA-sequencing**

533 Alignment and pre-processing of RNA-seq data, transcript normalization, and
534 subsequent analysis of pathway activity, and immune cell abundance have been
535 previously described[30].

536

537 **Gene signatures and the T cell-to-stroma enrichment score**

538 A list of 36 gene signatures representing immune and stromal resident cells and their
539 products was built from previously published resources (**Supplementary Table 2 and**
540 **Supplementary Data 3**). Normalized gene expression levels were median centered,
541 and the signature score was calculated as the mean expression of all genes per
542 signature. Hierarchical clustering of gene signatures (**Fig. 4**) showed that cluster one,
543 enriched for responders, had a high signature score for immune cells and a low
544 signature score for stromal resident cells and their products. Vice versa, cluster three
545 with only non-responders, had a low signature score for immune cells and a high
546 signature score for stromal resident cells and their products. Even though this result
547 extended earlier findings that signatures of immune *versus* stromal resident cells and
548 their products have differential predictive value, the contribution of individual signatures
549 to the identified cluster of patients may vary considerably. When applying hierarchical
550 clustering, we identified a group of signatures for T cells (Cytotoxic CD8 T cell, T cell

551 inflamed GEP, tGE8, T cell signature, IFN gamma, Immune gene signature and
552 chemoattractants) and stromal resident cell and products (Stromal signature,
553 Fibroblasts, EMT/stroma core genes, CAF, TBRS) with a highly similar transcriptomic
554 profile (**Supplementary Fig. 4**). In addition, these specific signatures also had high
555 discriminatory abilities reflected in high standard deviations across samples and
556 predictive values as shown by the AUC of ROC curves for response to pembrolizumab
557 (**Supplementary Table 3**). To assess and weigh the contribution of these 2 groups of
558 signatures, the overall mean of the selected signature scores for T cells and stromal
559 resident cells and products was calculated. These two metrics were considered to
560 represent the global signatures for T cells and stromal resident cells and products, and
561 at the same time filter out the noise that individual signatures may have. These 2 global
562 signature scores had independent predictive power for responders (T cells:
563 Coefficient=3.03; p=0.005) and non-responders (Stromal resident cells and products:
564 Coefficient=-2.40; p=0.010) according to multivariate logistic regression analysis.
565 Remarkably, the arithmetic difference between these 2 global signatures (T cells minus
566 stromal resident cells and products), which captures the concept that stromal resident
567 cells and their products may pose a barrier to T cells, showed a significantly improved
568 predictive value when compared to either single global signatures or individual gene
569 signatures (**Supplementary Table 3**). This new metric was named the T cell-to-stroma
570 enrichment (TSE) score because a positive TSE score points to an enrichment for T
571 cells, while a negative TSE score points to an enrichment for stromal resident cells and
572 their products. In fact, this metric emphasizes such enrichments as the normalized
573 gene expression data which are raw counts transformed on the log2 scale[38]. Finally,
574 we stratified patients into 3 groups according to their TSE score. The TSE score=0.5
575 was selected as cut-off with which the 3 groups of patients obtained resembled the

576 original clusters from **Fig. 4**. Patients with a TSE score ≥0.5 were considered to have
577 a positive TSE score, patients with a TSE score ≤-0.5 were considered to have a
578 negative TSE score and other patients were considered to have a neutral TSE score.
579 It is noteworthy that tumor purity does not act as a confounder for the TSE score. First,
580 tumor purity is negatively affected by the presence of non-tumor cells, which is alike
581 for T cells or resident stromal cells as evidenced by similar negative correlations
582 between tumor purity and either one of the global signatures (**Supplementary Fig.**
583 **S13**). Second, the TSE score automatically corrects for tumor purity since the former
584 is calculated per patient and inherently represents enrichments of either T cells or
585 resident stromal cells and their products.
586
587 **TCR repertoire**
588 RNA-seq data was processed with MiXCR v3.0.13[39] to estimate the TCR repertoire
589 (true) diversity and clonality. Samples with >100 total TCR reads were considered for
590 downstream analysis. The relative proportion (*R*) was used to group clonotype sizes
591 as follows: rare when only one read supported a clonotype; infrequent when *R*<1%;
592 frequent when *R*=1%-10%; and hyper-frequent when *R*>10%.
593
594 **Immunofluorescence staining, imaging and analysis of T cell and stromal**
595 **markers**
596 We performed immunofluorescence stainings using whole slides of 20 patient samples
597 of which paired RNA-seq data was available (TSE positive, n=7; TSE neutral, n=8;
598 TSE negative, n=5). We stained for T cells (CD4 and CD8 T cells) and stromal cells
599 (FAP and PDPN) using markers that were considered representative for the gene
600 signatures used to build the TSE score at RNA level. To this end, a second biopsy,

601 which was obtained from the same lesion and collected at the same time as the first
602 biopsy, was formalin-fixed and paraffin-embedded. Stainings for DAPI, CD3 and CD8
603 were obtained from multiplexed immunofluorescence performed using OPAL reagents
604 (Akoya Biosciences, Marlborough, MA, USA) on 4 µm sections. Slides were scanned
605 and images were obtained using VECTRA 3.0 (Akoya Biosciences), after which at least
606 4 stamps (regions of interest; stamp size: 671x500 μm^2; resolution: 2pixes/µm; pixel
607 sixe: 0.5x0.5μm^2) were set in non-necrotic areas to cover >90% of tissue area. Images
608 were spectrally unmixed using inForm® software (v2.4.8; Akoya Biosciences) to
609 visualize the above markers as well as autofluorescence. Subsequently, images were
610 manually analyzed using an in-house generated python-based image interface as
611 described previously[35]. CD3+CD8+ cells were phenotyped as CD8 cells, and
612 CD3+CD8- cells were phenotyped as CD4 cells, and their densities were calculated by
613 dividing the number of cells by the tissue area. In two cases (one TSE positive and one
614 TSE negative), quantification of CD4 and CD8 cells failed. In addition, consecutive
615 sections were stained for FAP (EPR20021, Abcam) – FAM (#760-243, Ventana),
616 PDPN (D2-40, Cell Marque) – Cy5 (Roche Applied Science), and DAPI. These slides
617 were scanned using a Zeiss microscope (Zeiss) and the regions of interest
618 corresponding to the above T cell markers were exported using the Qupath software
619 (v0.4.1). Image analysis was again performed using an in-house generated python-
620 based user interface[35]. In short, tissue areas were determined by performing gaussian
621 blurring on the DAPI channel with a kernel size of 30 pixels, and manually thresholding
622 this image. The thresholding for FAP and PDPN-positive areas was also performed
623 manually using raw images corrected for background signal. Background correction
624 for FAP images was performed via subtraction of uniform filtered images with a filter
625 size of 500 from the original images. As the PDPN intensity was relatively uniform,

626 background correction was not performed. Percentages of marker-positive areas were
627 determined by dividing the areas positive for either marker by the total tissue area.
628 Outcomes of individual T cell and stromal markers were used to generate a TSE-
629 protein score in analogy to the TSE-RNA score. Values of the 4 protein markers were
630 log10 transformed as log10(1+value), after which the stromal markers (FAP, PDPN)
631 were subtracted from the T cell markers (CD4, CD8).
632

633 **Statistical analysis**

634 Analyses were performed using the platform R v4.1.0[40]. The Fisher's exact test was
635 used for comparison of categorical values between groups. The Wilcoxon-rank sum
636 test and the Kruskal-Wallis test by ranks were used for comparison of 2 or >2 groups
637 with continuous variables, respectively. DeLong's and log-rank tests were used for
638 comparing receiver operating characteristics (ROC) and Kaplan-Meier survival curves,
639 respectively. For multivariate analyses, the Cox proportional hazards regression
640 analysis and the logistic regression analysis were applied.
641

642 **Data availability**

643 WGS, RNA-seq and clinical data are available through the Hartwig Medical Foundation
644 at https://www.hartwigmedicalfoundation.nl, under request number DR-176. Source
645 data for figures, including quantification of protein markers from tissue staining, are
646 provided with this paper.

647

648 **Code availability**

649 The pipeline for alignment and pre-processing of WGS data developed by the
650 Hartwig Medical Foundation are deposited at

651 https://github.com/hartwigmedical/hmftools. The script to calculate the TSE score

652 from RNA normalized counts is available at

653 https://github.com/ANakauma/TSEscore_ICIs.

654

References

1. Bellmunt J, de Wit R, Vaughn DJ, et al: Pembrolizumab as Second-Line Therapy for Advanced Urothelial Carcinoma. N Engl J Med 376:1015-1026, 2017
2. Rijnders M, de Wit R, Boormans JL, et al: Systematic Review of Immune Checkpoint Inhibition in Urological Cancers. Eur Urol 72:411-423, 2017
3. Fradet Y, Bellmunt J, Vaughn DJ, et al: Randomized phase III KEYNOTE-045 trial of pembrolizumab versus paclitaxel, docetaxel, or vinflunine in recurrent advanced urothelial cancer: results of > 2 years of follow-up. Ann Oncol, 2019
4. Balar AV, Castellano D, O'Donnell PH, et al: First-line pembrolizumab in cisplatin-ineligible patients with locally advanced and unresectable or metastatic urothelial cancer (KEYNOTE-052): a multicentre, single-arm, phase 2 study. Lancet Oncol 18:1483-1492, 2017
5. Balar AV, Galsky MD, Rosenberg JE, et al: Atezolizumab as first-line treatment in cisplatin-ineligible patients with locally advanced and metastatic urothelial carcinoma: a single-arm, multicentre, phase 2 trial. Lancet 389:67-76, 2017
6. Lee HH, Ham WS: Perioperative immunotherapy in muscle-invasive bladder cancer. Translational Cancer Research 9:6546-6553, 2020
7. Ghate K, Amir E, Kuksis M, et al: PD-L1 expression and clinical outcomes in patients with advanced urothelial carcinoma treated with checkpoint inhibitors: A meta-analysis. Cancer Treatment Reviews 76:51-56, 2019
8. Powles T, Csőszi T, Özgüroğlu M, et al: Pembrolizumab alone or combined with chemotherapy versus chemotherapy as first-line therapy for advanced urothelial carcinoma (KEYNOTE-361): a randomised, open-label, phase 3 trial. The Lancet Oncology 22:931-945, 2021
9. Galsky MD, Arija JÁA, Bamias A, et al: Atezolizumab with or without chemotherapy in metastatic urothelial cancer (IMvigor130): a multicentre, randomised, placebo-controlled phase 3 trial. The Lancet 395:1547-1557, 2020
10. Rijnders M, van der Veldt AAM, Zuiverloon TCM, et al: PD-L1 Antibody Comparison in Urothelial Carcinoma. Eur Urol 75:538-540, 2019
11. Powles T, Walker J, Andrew Williams J, et al: The evolving role of PD-L1 testing in patients with metastatic urothelial carcinoma. Cancer Treat Rev 82:101925, 2020
12. Cristescu R, Mogg R, Ayers M, et al: Pan-tumor genomic biomarkers for PD-1 checkpoint blockade-based immunotherapy. Science 362, 2018
13. Gupta S, Huang RSP, Stanke J, et al: Tumor mutational burden as a predictive biomarker for immune checkpoint inhibitor versus chemotherapy benefit in first-line metastatic urothelial carcinoma: A real-world study. Journal of Clinical Oncology 40:547-547, 2022
14. Marabelle A, Fakih M, Lopez J, et al: Association of tumour mutational burden with outcomes in patients with advanced solid tumours treated with pembrolizumab: prospective biomarker analysis of the multicohort, open-label, phase 2 KEYNOTE-158 study. Lancet Oncol 21:1353-1365, 2020
15. FDA Approves Pembrolizumab for Adults and Children With Tumor Mutational Burden–High Solid Tumors, 2020
16. Rosenberg JE, Hoffman-Censits J, Powles T, et al: Atezolizumab in patients with locally advanced and metastatic urothelial carcinoma who have progressed following treatment with platinum-based chemotherapy: a single-arm, multicentre, phase 2 trial. Lancet 387:1909-20, 2016
17. Tumeh PC, Harview CL, Yearley JH, et al: PD-1 blockade induces responses by inhibiting adaptive immune resistance. Nature 515:568-71, 2014
18. Powles T, Kockx M, Rodriguez-Vida A, et al: Clinical efficacy and biomarker analysis of neoadjuvant atezolizumab in operable urothelial carcinoma in the ABACUS trial. Nature Medicine 25:1706-1714, 2019
19. Sharma P, Retz M, Siefker-Radtke A, et al: Nivolumab in metastatic urothelial carcinoma after platinum therapy (CheckMate 275): a multicentre, single-arm, phase 2 trial. Lancet Oncol 18:312-322, 2017
20. Mariathasan S, Turley SJ, Nickles D, et al: TGFβ attenuates tumour response to PD-L1 blockade by contributing to exclusion of T cells. Nature 554:544-548, 2018
21. Bagaev A, Kotlov N, Nomie K, et al: Conserved pan-cancer microenvironment subtypes predict response to immunotherapy. Cancer Cell 39:845-865.e7, 2021
22. Teo MY, Seier K, Ostrovnaya I, et al: Alterations in DNA Damage Response and Repair Genes as Potential Marker of Clinical Benefit From PD-1/PD-L1 Blockade in Advanced Urothelial Cancers. Journal of Clinical Oncology 36:1685-1694, 2018
23. Mendelaar PAJ, Robbrecht DGJ, Rijnders M, et al: Genome-wide aneuploidy detected by mFast-SeqS in circulating cell-free DNA is associated with poor response to pembrolizumab in patients with advanced urothelial cancer. Molecular Oncology n/a, 2022
24. Vandekerkhove G, Lavoie J-M, Annala M, et al: Plasma ctDNA is a tumor tissue surrogate and enables clinical-genomic stratification of metastatic bladder cancer. Nature Communications 12:184, 2021
25. Snyder A, Nathanson T, Funt SA, et al: Contribution of systemic and somatic factors to clinical response and resistance to PD-L1 blockade in urothelial cancer: An exploratory multi-omic analysis. PLoS Med 14:e1002309, 2017

26. Galsky M, Saci A, Szabo PM, et al: Nivolumab in Patients with Advanced Platinum-Resistant Urothelial Carcinoma: Efficacy, Safety, and Biomarker Analyses with Extended Follow-up from CheckMate 275. Clin Cancer Res, 2020

27. Powles T, Sridhar SS, Loriot Y, et al: Avelumab maintenance in advanced urothelial carcinoma: biomarker analysis of the phase 3 JAVELIN Bladder 100 trial. Nature Medicine 27:2200-2211, 2021

28. Bellmunt J, de Wit R, Fradet Y, et al: Putative Biomarkers of Clinical Benefit With Pembrolizumab in Advanced Urothelial Cancer: Results from the KEYNOTE-045 and KEYNOTE-052 Landmark Trials. Clinical Cancer Research:OF1-OF11, 2022

29. Priestley P, Baber J, Lolkema MP, et al: Pan-cancer whole-genome analyses of metastatic solid tumours. Nature 575:210-216, 2019

30. Nakauma-González JA, Rijnders M, van Riet J, et al: Comprehensive Molecular Characterization Reveals Genomic and Transcriptomic Subtypes of Metastatic Urothelial Carcinoma. European Urology 81:331-336, 2022

31. Saraiva M, Vieira P, O'Garra A: Biology and therapeutic potential of interleukin-10. Journal of Experimental Medicine 217:e20190418, 2019

32. Wang L, Saci A, Szabo PM, et al: EMT- and stroma-related gene expression and resistance to PD-1 blockade in urothelial cancer. Nature Communications 9:3503, 2018

33. Aran A, Garrigós L, Curigliano G, et al: Evaluation of the TCR Repertoire as a Predictive and Prognostic Biomarker in Cancer: Diversity or Clonality? Cancers 14:1771, 2022

34. Kidman J, Principe N, Watson M, et al: Characteristics of TCR Repertoire Associated With Successful Immune Checkpoint Therapy Responses. Frontiers in Immunology 11, 2020

35. Rijnders M, Balcioglu HE, Robbrecht DGJ, et al: Anti-PD1 efficacy in metastatic urothelial cancer patients associates with intra-tumoral juxtaposition of T helper-type 1 and CD8+ T-cells. Clin Cancer Res, 2021

36. van Dessel LF, van Riet J, Smits M, et al: The genomic landscape of metastatic castration-resistant prostate cancers reveals multiple distinct genotypes with potential clinical impact. Nature Communications 10:1-13, 2019

37. Stephens PJ, Tarpey PS, Davies H, et al: The landscape of cancer genes and mutational processes in breast cancer. Nature 486:400-404, 2012

38. Love MI, Huber W, Anders S: Moderated estimation of fold change and dispersion for RNA-seq data with DESeq2. Genome Biology 15:550-550, 2014

39. Bolotin DA, Poslavsky S, Mitrophanov I, et al: MiXCR: Software for comprehensive adaptive immunity profiling, Nature Publishing Group, 2015, pp 380-381

40. Team RC: R Core Team (2017). R: A language and environment for statistical computing. R Foundation for Statistical Computing, Vienna, Austria. URL http://www.R-project.org/.R Foundation for Statistical Computing-R Foundation for Statistical Computing, 2017

41. Yu G, He QY: ReactomePA: An R/Bioconductor package for reactome pathway analysis and visualization. Molecular BioSystems 12:477-479, 2016

42. Wilkerson MD, Hayes DN: ConsensusClusterPlus: A class discovery tool with confidence assessments and item tracking. Bioinformatics 26:1572-1573, 2010

759 **Acknowledgements**

760 This publication and the underlying research are partly facilitated by Hartwig Medical
761 Foundation and the Center for Personalized Cancer Treatment (CPCT) which have
762 generated and made available data for this research. We thank all local principal
763 investigators and the nurses of all contributing centers for their help with patient
764 recruitment. We are particularly grateful to all participating patients and their families.
765 Funding for this research was provided by The Dutch Research Council (NWO) under
766 grant-number 848050012 and by Merck Sharp & Dohme.

767

768 **Author contributions**

769 Conceptualization: MPL, RD, DGJR; Methodology: MR, JAN, AAMO, MPL, RD; Data
770 analysis: JAN, HEB, AGJ; Data interpretation: MPL, RD, DGJR, MR, JAN; Clinical
771 data collection and interpretation: MR, MPL, RD, DGJR, MJBA, JLB, PH, MSvdH,
772 BES, GJLHvL, NM, JV, HMW, RdW, aAAMvdV. Immunohistochemistry: AAMO, HEB,
773 GJLHvL, MR; Writing – Original Draft: All authors; Writing – Review & Editing: MR,
774 JAN, MPL, RD. All authors read and approved the final manuscript.

775

776 **Authors' disclosures of potential conflicts of interest**

777 Martijn P. J. Lolkema has received research support from JnJ, Sanofi, Astellas and
778 MSD, and consultancy fees from Incyte, Amgen, JnJ, Bayer, Servier, Roche, INCa,
779 Pfizer, Sanofi, Astellas, AstraZeneca, Merck Sharp & Dohme, Novartis, Julius Clinical
780 and the Hartwig Medical Foundation (all paid to the Erasmus MC Cancer Institute).
781 Debbie G.J. Robbrecht has received research support from Treatmeds and
782 consultancy fees from Bristol-Myers Squibb, Bayer, AstraZeneca, Merck, Pfizer (all
783 paid to the Erasmus MC Cancer Institute).

784 Ronald de Wit has received consultancy fees from Sanofi, Merck, Astellas, Bayer,
785 Hengrui and Orion, speaker fees from Sanofi and Astellas, research support from
786 Sanofi and Bayer (all paid to the Erasmus MC Cancer Institute).
787 Astrid A.M. van der Veldt has received consultancy fees from for BMS, MSD, Merck,
788 Novartis, Roche, Sanofi, Pierre Fabre, Ipsen, Eisai, Pfizer (all paid to the Erasmus MC
789 Cancer Institute).
790 Michiel S. van der Heijden has received research support from Bristol-Myers Squibb,
791 AstraZeneca and Roche, and consultancy fees from Bristol-Myers Squibb, Merck
792 Sharp & Dohme, Roche, AstraZeneca, Seattle Genetics and Janssen (all paid to the
793 Netherlands Cancer Institute).
794 Joost L. Boormans has received research support from Decipher Biosciences and
795 Merck Sharp & Dohme, and consultancy fees from Merck Sharp & Dohme, Eight
796 Medical, Ambu, APIM therapeutics, Bristol-Myers Squibb, Astellas Roche and Janssen
797 (all paid to the Erasmus MC Cancer Institute).
798 Niven Mehra has received research support from Astellas, Janssen, Pfizer, Roche and
799 Sanofi Genzyme, and consultancy fees from Roche, MSD, BMS, Bayer, Astellas and
800 Janssen (all paid to the Radboud University Medical Center).
801 Hans M. Westgeest has received consultancy fees from Roche and Astellas (all paid
802 to the Amphia hospital, Breda).
803 Paul Hamberg has received consultancy fees from Astellas, Merck Sharp & Dohme,
804 Pfizer AstraZeneca, Bristol-Myers Squibb and Ipsen (all paid to the Franciscus
805 Gasthuis & Vlietland Hospital, Rotterdam/Schiedam).
806 Maureen J.B. Aarts has received advisory board / consultancy honoraria from Amgen,
807 Bristol Myers Squibb, Novartis, MSD-Merck, Merck-Pfizer, Pierre Fabre, Sanofi,

Astellas, Bayer, research grants from Merck-Pfizer (all paid to Maastricht UMC+ Comprehensive Cancer Center).

Geert J.L.H. van Leenders has received research grants from Roche and AstraZenaca, and has been member of advisory boards of Roche and Merck (all paid to the Erasmus MC Cancer Institute).

Reno Debets has received research support from MSD and Bayer, personal fees from Bluebird Bio, Genticel, other support from Pan Cancer T outside the submitted work (all paid to the Erasmus MC Cancer Institute), and is listed as inventor for European patent application no's. 21152822.9 and 21184727.2 (pending to Erasmus MC).

Maud Rijnders, J. Alberto Nakauma-González, Alberto Gil-Jimenez, Jens Voortman, Astrid A. M. Oostvogels and Hayri E. Balcioglu declare no competing interests.